Astron. Astrophys. 325, 685–692 (1997)

ASTRONOMY
AND
ASTROPHYSICS

Young Stellar Objects in Lynds 1641: a submillimetre continuum study

A. Zavagno[1,2], **S. Molinari**[1,3], **E. Tommasi**[1], **P. Saraceno**[1], **and M. Griffin**[4]

[1] CNR-Istituto di Fisica dello Spazio Interplanetario, Casella Postale 27, I-00044 Frascati (Rome), Italy
[2] Observatoire de Marseille, 2 Place Le Verrier, F-13248 Marseille Cedex 4, France (Zavagno@obmara.cnrs-mrs.fr)
[3] CNR-Istituto di Radioastronomia, v. Gobetti 101, I-40129 Bologna, Italy
[4] Queen Mary and Westfield College, Physics Dept., Mile End Rd., London E1 4NS, UK

Received 23 September 1996 / Accepted 2 April 1997

Abstract. We present observations of the 350 μm – 1.3 mm continuum emission of a sample of ten Class I young stellar objects in the Lynds 1641 (L1641) molecular cloud. These observations, together with IRAS data, are used to determine and discuss the properties of the circumstellar dust. We interpret these results in an evolutionary scheme and we find that, in our sample, the exponent of the dust opacity law, β, seems to increase with time.

Key words: stars: pre-main-sequence – stars: circumstellar matter – interstellar medium: dust – radio continuum: stars

1. Introduction

Young stellar objects (YSOs) are characterized by being deeply embedded in the gas and dust of their parent clouds. During the protostellar phase, the mass of the circumstellar material decreases in part due to accretion onto the central star, in part because of outflow. Because the submillimetre range is sensitive to the cold circumstellar material, it is an ideal domain for studying the first steps of stellar evolution (Cabrit & André 1991; Reipurth et al. 1993; André & Montmerle 1994; Henning et al. 1994).

André et al. (1993) and Saraceno et al. (1996) suggested that the bolometric ($L_{\rm bol}$) and the millimetre ($L_{1.3\,\rm mm}$) luminosities can provide a very useful tool for tracing the different phases of protostellar evolution. This evolution is, in fact, determined by two factors: the central object's mass which defines $L_{\rm bol}$ and the circumstellar mass which is proportional to the millimetre flux since the dust can be assumed to be optically thin in this wavelength range. André et al. (1993) and Saraceno et al. (1996) assumed that the dust characteristics are constant during the pre-main-sequence evolution. Nevertheless, dust properties may change during protostellar evolution (Seab 1987; Cardelli et al. 1989). Starting from these considerations, Dent et al. (1995), using a submillimetre colour-colour diagram on a sample of young sources in different evolutionary stages, found that β, the exponent of the dust opacity law, seems to change with time, suggesting an evolution of dust properties.

In this work, we discuss the possibility and the impact of a change in dust properties during the evolution. We present 350 μm to 1.3 mm continuum observations of the ten most luminous ($L_{\rm bol}$ <200 $L_{\odot}$) Class I sources (Lada 1987) in L1641, selected from the work of Strom et al. (1989, hereafter SNS). These sources are highly embedded, associated with dense cores and outflow activity. They cover a large range of ($L_{\rm bol}/L_{1.3\,\rm mm}$) values and are well suited to the purpose of this work. For these objects, we determine dust properties and masses and we attempt to identify a possible evolution of dust characteristics.

The giant molecular cloud L1641 is located in the southern part of the Ori A molecular cloud at a distance of 480 pc (SNS). This cloud and its associated IR sources have been extensively studied (SNS; Chen et al. 1993a,b; Chen & Tokunaga 1994). The outflow activity in this cloud has been studied by Morgan & Bally (1991) and by Morgan et al. (1991). Individual YSOs in this cloud have been studied by Davis & Eislöffel (1995), McMullin et al. (1994), Morgan et al. (1990) and Myers et al. (1987).

Sect. 2 presents the observations and Sect. 3 deals with the data analysis and results. The possible change of β with time is discussed in Sect. 4. Finally, the main conclusions are drawn in Sect. 5. A discussion of individual sources is presented in the Appendix.

2. Submillimetre observations

We carried out continuum observations from 350 μm to 1.3 mm with the UKT14 common user bolometer receiver (Duncan et al. 1990) on the 15-m James Clerk Maxwell Telescope (JCMT) on Mauna Kea, Hawaii, in October 1993 and March 1994. The 65 mm aperture was used. The FWHM beamwidth varied be-

Send offprint requests to: A. Zavagno

tween 17″ and 20″, depending on the filter. A chop throw of 60″ was used with a chopping frequency of 7.8 Hz. Calibration was mainly referred to OMC1 (which, being close to L1641, had a similar air mass) and checked with secondary standards from the JCMT calibration source catalogue (Sandell 1994).

The observations were carried out by pointing at the coordinates given by Chen & Tokunaga (1994; see their Table 5) which correspond to the near IR counterparts of the IRAS sources (for VLA1, not detected in the near IR, we used the VLA coordinates). Then a small map was carried out at 800 μm in order to define the peak emission position (given in columns 2 and 3 of Table 1). At this position, photometry at 1.3 mm, 1.1 mm, 800 μm and, when possible, at 350 and 450 μm was carried out.

For all sources except S22 and S32, for which the displacement is less than 18″, the submillimetre emission peak has been found within 10″ (0.022 pc) of the reddest near IR source. This coincidence (within the JCMT spatial resolution) proves that the objects are very young and still embedded in their parental cloud. Table 1 lists the results of our observations. Column 1 gives the source name (given by SNS). Columns 2 and 3 give the coordinates of the aperture center. The bolometric luminosities (and uncertainties) determined from our calculations (see Sect. 3.1) are given in column 4. The outflow status, outflow (OF) or non detected flow (NDF) given in column 5, refers to the Saraceno et al. (1996) classification. For the VLA1 outflow, we refer to Correia et al. (1996). Columns 6 to 10 give, in janskys, the submillimetre fluxes from 350 μm to 1.3 mm, together with the total error (which includes statistical, photometric and absolute calibration uncertainties estimated at 10% level). No corrections for spectral beam size variations have been applied as they are negligible compared to total flux errors.

3. Data analysis and results

3.1. Luminosity determination

We calculated the bolometric luminosity of the observed sources by integrating the continuum emission between 12 μm and 1.3 mm using the IRAS fluxes from SNS and our submillimetre measurements. Emission outside the 12 μm – 1.3 mm range does not significantly contribute to the total luminosity (see also Reipurth et al. 1993) because, for Class I sources, the spectral energy distribution is sharply peaked around 100 μm (see Fig. 1 and Lada 1991).

For the IRAS fluxes we adopted the SNS values because they used one-dimensional co-adds and determined more accurate fluxes than those of the IRAS Point Source Catalog (1988; PSC). Moreover, the PSC gives upper limits for six of the sources. Chen et al. (1993b) also determine IR fluxes using co-added images and aperture photometry. They determine fluxes with very small uncertainties (4% at 100 μm for four sources of our sample). In spite of this, we have discarded these fluxes because we find that they do not fit the overall observed continuum. Luminosity errors given in Table 1 take into account all the errors in flux determination between 12 μm and 1.3 mm. The results of our calculations are given in column 4 of Table 1. Our luminosity determinations generally agree, to within the errors, with those of Chen et al. (1993b).

3.2. The circumstellar dust

In order to obtain the mass, temperature and β of the circumstellar dust, we used the formula (Hildebrand 1983) which, in an optically thin case, expresses the observed flux, $f(\lambda)$, as

$$f(\lambda) = \frac{M}{D^2}\ \kappa(\lambda)\ B(\lambda,T) \quad \text{with} \quad \kappa(\lambda) = \kappa_0 \left(\frac{250\ \mu\text{m}}{\lambda}\right)^{\beta} \quad (1)$$

where D is the cloud distance, $B(\lambda,T)$ is the Planck function, M is the total mass, assuming a gas-to-dust ratio of 100, and κ_0=κ(250 μm)=0.1 cm^2/g is the dust opacity (Hildebrand 1983). In Sect. 3.4 we discuss the value of κ_0.

The optically thin regime can be assumed at submillimetre wavelengths because dust emission is optically thin up to column densities of $N_{\rm H_2} \simeq 10^{26}$ cm^{-2} (Hildebrand 1983). We have checked that the estimated values for dust opacity verify this assumption.

We used a least-squares fit method to determine the best values of T, β and M to fit, with Eq. 1, the far IR and submillimetre data. The use of the far IR fluxes at 60 and 100 μm in this procedure is crucial, as it defines the emission peak and then greatly influences the obtained dust temperature. For all sources, started from the same initial set of parameters (T=20 K, β=1, M=0.1 $M_\odot$) we computed the flux $f(\lambda)$ and the quantity

$$\chi^2 = \sum_i \left(\frac{F_i - f_i}{\Delta F_i}\right)^2 \quad (2)$$

where, for each wavelength i, f_i is the flux value computed from Eq. 1, F_i and ΔF_i are the observed ones and their error (from Table 1). One of the three parameters was changed in step of 10% until a minimum value of χ^2 was reached. Then, the same process was repeated sequencially for the two other parameters. When a minimum value of χ^2 is reached with these three parameters, we decrease the step by a factor 1.25 and reiterate the process described here above. At each decrease of the step, the best-fit procedure started with the values that minimised χ^2 at the end of the precedent cycle. Convergence was reached after a maximum of 20 iterations. We checked that, changing the initial values and the order of the parameters does not change the result.

In order to evaluate the uncertainties associated with the parameters, mainly due to the errors on IR fluxes, two different fits have been obtained. The first (second) curve passes through the minimum (maximum) flux at 60 μm and the maximum (minimum) flux at 100 μm, both compatible with a 1σ error in these fluxes. Therefore, two limiting values are given for each parameter together with the best-fit one.

Fig. 1 presents the observed submillimetre spectra together with the best-fit result (solid line) for nine of our ten sources. S31 was not considered because SNS did not obtained IR fluxes for this source. In Fig. 1 we also show the spectral energy distribution of two T Tauri stars (Class II sources; IR and submillimetre

Table 1. Sources properties and observed submillimetre fluxes

Name	α (1950)	δ (1950)	L_{bol} ($L_\odot$)	OF/ NDF	350 μm 18.5″	450 μm 17.5″	800 μm 16.8″	1.1 mm 18.5″	1.3 mm 19.5″
S06	$5^h\,33^m\,52\overset{s}{.}7$	−06°24′02″	167 (33)	OF	53.5 (19.5)	30.6 (9.1)	5.14 (1.13)	1.99 (0.14)	1.29 (0.14)
S11	33 59.4	−06 26 44	45 (2)	OF	12.5 (3.6)	8.07 (1.69)	1.45 (0.11)	0.49 (0.05)	0.44 (0.05)
S22	34 09.2	−06 40 18	32 (10)	OF		6.36 (1.29)	1.26 (0.14)	0.452 (0.053)	0.547 (0.107) **
S31	33 59.1	−06 46 29	55 (12.5) *	NDF	6.52 (2.10)	3.69 (0.74)	0.763 (0.118)	0.287 (0.036)	0.220 (0.031)
S32	33 52.9	−06 47 12	77 (15)	OF		7.81 (1.73)	1.29 (0.14)	0.45 (0.06)	0.323 (0.051)
S55	38 02.7	−07 28 59	175 (14)	OF		6.12 (1.15)	0.884 (0.098)	0.371 (0.039)	0.261 (0.036)
S59	37 31.1	−07 31 59	100 (15)	OF	34.7 (10.5)	16.3 (2.8)	3.19 (0.32)	1.23 (0.07)	0.852 (0.122)
S72	39 00.2	−07 56 33	15 (7.5)	NDF			0.877 (0.140)	0.318 (0.051)	0.169 (0.042)
S85	38 24.8	−08 08 25	15.5 (3)	OF			0.799 (0.118)	0.314 (0.037)	0.233 (0.035)
VLA1	33 57.01	−06 47 55	21 (6)	OF	23.0 (6.3)	12.87 (2.15)	2.64 (0.37)	0.923 (0.073)	0.785 (0.143) **

Fluxes (and total errors) are given in Jy
* upper limit (see Appendix)
** 1.3mm excess (see Appendix)

Table 2. Obtained parameters (isothermal and isodense approximation)

Name	β	$\Delta\beta$	$\overline{T}$ (K)	$\Delta\overline{T}$ (K)	$\overline{M}$ ($M_\odot$)	$\Delta\overline{M}$ ($M_\odot$)	$\tau_{60\ \mu m}$	$\tau_{100\ \mu m}$
S06	1.57	1.51 - 1.6	30.2	29.5 - 31	3.9	3.5 - 4.3	0.45	0.20
S11	1.24	1.16 - 1.44	28.8	26 - 30	0.71	0.6 - 1.06	0.05	0.03
S22	1.51	1.08 - 1.64	28.6	27 - 35	0.84	0.38 - 1.08	0.09	0.04
S32	1.64	1.56 - 1.72	33.5	32 - 35	0.87	0.74 - 1.02	0.11	0.05
S55	1.68	1.47 - 1.87	39.1	35 - 45	0.49	0.32 - 0.72	0.05	0.02
S59	1.26	1.16 - 1.35	35.7	34 - 37.5	1.24	1 - 1.5	0.09	0.05
S72	1.4	1.1 - 1.54	29	27 - 33	0.49	0.28 - 0.66	0.04	0.02
S85	1.21	1.12 - 1.29	32	31 - 33.5	0.35	0.29 - 0.4	0.02	0.01
VLA1	1.25	1.06 - 1.37	28.4	26.5 - 31	1.2	0.87 - 1.61	0.1 (50 μm)	0.05

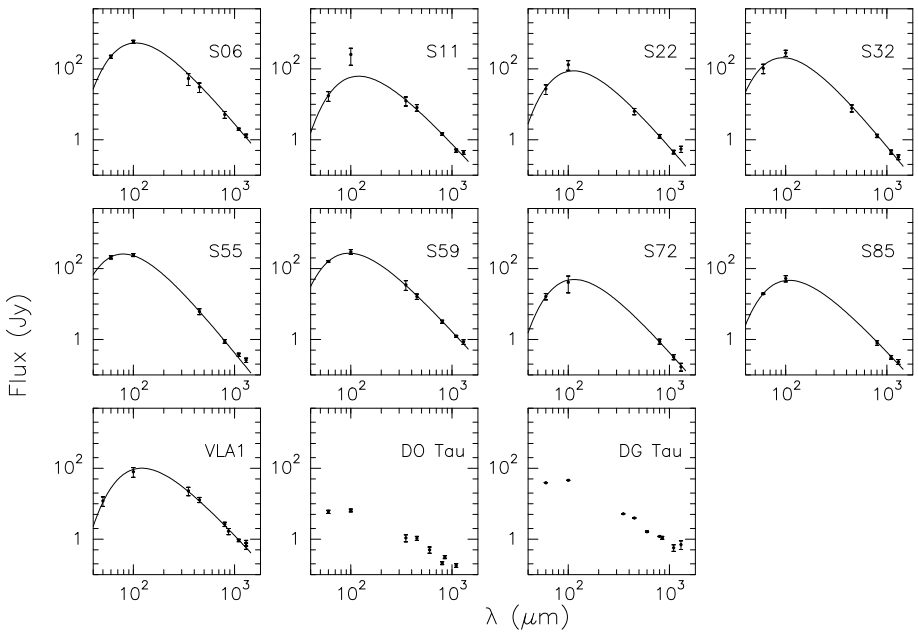

Fig. 1. Observed continuum emission from 60 μm to 1.3 mm for 9 sources of our sample. The solid line represents the best-fit result. The continuum emission of two T Tauri stars is also shown for comparisons

measurements are from the IRAS-PSC 1988 and Mannings & Emerson 1994, respectively). There is a clear difference between the SEDs of Class I and Class II objects, probably due to differences in the geometry of the emitting regions (probably disk-dominant in case of T Tauri stars, Mannings & Emerson 1994). Therefore, because the Hildebrand formalism assumes a spherical geometry, no fit is obtained for these two T Tauri stars.

Fig. 1 shows that we can fairly well reproduce the continuum emission observed for our sources between 60 μm and 1.3 mm using a single temperature greybody. The only noticeable exception is for S11 whose fit is too low to agree with the observed 100 μm flux. We suspect that this flux is overestimated because, taking the mean value of $\log(F_{60}/F_{100})$= -0.4 derived for Class I sources in L1641 (Chen et al. 1993b), we find for S11 an "expected" 100 μm flux of 60 Jy that agrees with our fit.

The parameters (β, M and T) obtained with these assumptions are presented in Table 2 together with the values of the optical depth at 60 and 100 μm .

Columns 2 to 7 present the β values, dust temperature and the total circumstellar mass, along with limiting values (obtained with the two extreme fits; see above). For each source, the highest β value is associated with the highest mass and the lowest temperature. Columns 8 and 9 present, respectively, the values of the optical depth at 60 and 100 μm obtained using the relation between the optical depth and the dust opacity law

$$\tau(\lambda) = N\kappa(\lambda) \quad (3)$$

where N is the dust column density (the mass divided by the beam area at the cloud distance) and κ is the dust opacity.

The temperatures are in the range 26 - 40 K as expected for YSOs, with a continuum emission that peaks around 100 μm (see also Reipurth et al. 1993; André & Montmerle 1994; Henning et al. 1994). This temperature can be interpreted as the mean dust temperature (Walker et al. 1990), mass-averaged (Henning 1983) over the envelope. The mass values are in the range 0.5 - 4 $M_\odot$. Hence we are dealing with cold objects of relatively low mass. We note that the masses are function of the value chosen for κ_0; a higher κ_0 would lead to a smaller mass, but κ_0 is not well known (see Sect. 3.4).

We find β in the range 1.1 – 1.9. This range represents the very extreme limits. The value of β should characterize the dust type that constitutes the envelope. However, opacity effects can weaken or cancel the link between the slope and the intrinsic dust properties (see Reipurth et al. 1993). This point is crucial for young sources, as opacity effects could lead to a "look-alike" flatter spectrum as observed for the Class 0 source HH24MMS (Ward-Thompson et al. 1995). Using Eq. 3, we verify that the optical depth is below unity both at 60 and 100 μm for all sources (see Table 2). Therefore opacity effects should not influence the parameter determinations.

Table 3. Spherical model results

Name	$T_{\rm ext}$	$\overline{T}$	$\rho_{\rm ext}$	M	$\overline{M}$
	(K)		(g/cm^3)	($M_\odot$)	
S06	24	30.2	2.3 10^{-20}	3.47	3.9
S11	21	28.8	5 10^{-21}	0.71	0.71
S22	21	28.6	6 10^{-21}	0.9	0.84
S32	26	33.5	7.5 10^{-21}	1	0.87
S55	26	39.1	6 10^{-21}	0.87	0.49
S59	26	35.7	1.1 10^{-20}	1.5	1.24
S72	21	29.0	4 10^{-21}	0.6	0.49
S85	24	32.0	2.8 10^{-21}	0.4	0.35
VLA1	21	28.4	9 10^{-21}	1.35	1.2

3.3. Validity of the approach

In order to see possible limitations arising from the adopted assumption of a unique dust temperature and density (as implied by the use of Eq. 1) we developed a spherical model assuming a power law distribution of temperature and density

$$\rho(r) = \rho_{\rm ext} \left(\frac{r}{r_{\rm ext}}\right)^{-p} \quad \text{and} \quad T(r) = T_{\rm ext} \left(\frac{r}{r_{\rm ext}}\right)^{-q} \quad (4)$$

where $T_{\rm ext}$ and $\rho_{\rm ext}$ represent, respectively, the dust temperature and density at the external radius ($r_{\rm ext}$) of the envelope.

In Eq. 4 we fix the density and temperature exponents p and q to 1.5 and 0.3 respectively, as expected in case of free-fall collapse (Adams 1991). We also fix the exponent β of the extinction law to the values obtained using Eq. 1 (see Table 2). This assumption should be correct as the main part of the far IR and submillimetre emission comes from the external shells where the temperature variation is weak. Therefore, possible variation of β due to temperature variation in the envelope should also be weak.

The continuum emission of each shell is computed taking into account its position in the envelope and the relative extinction. We verify that the envelope remains optically thin at the considered wavelengths. The total mass is then calculated, integrating the density over the total volume between the inner and outer radius of the envelope, fixed as follows: the outer radius ($r_{\rm ext}$) is fixed at 0.02 pc, which corresponds to the free-fall radius for a mean sound speed of 0.2 km/s and an age of 10^5 years, as expected from the star formation models. This age is in agreement with the upper limit of 3 10^6 years and the outflow dynamical time which is about 5 10^4 years for these objects (SNS). An external radius of 0.02 pc at a distance of 480 pc correspond to 10″, nearly half of the JCMT beam. Stopping the integration at this radius implies that the residual emission detected in the beam is subtracted by the chopping technique.

The inner radius is computed by fitting the data of each source with Eq. 4 and corresponds to the radius where the dust destruction temperature ($T_{\rm in}$=1500 K) is reached.

The free parameters of our model are the external temperatures and densities. The results are given in Table 3.

The values of $T_{\rm ext}$ and $\rho_{\rm ext}$ are, respectively, in the range 21 to 26 K and 10^5 to 10^6 cm^{-3}, in good agreement with the values

obtained for the L1641 cloud (15 to 30 K and 10^2 to 10^7 cm^{-3}; Sakamoto et al. 1994).

The masses obtained by integrating the density profile over the envelope is generally about 20% higher than the ones obtained assuming a unifor density and isothermal envelope. This may be due to the contribution of the higher density central regions of the envelope. On the other hand, the external temperatures $T_{\rm ext}$ estimated with the shell model are on average 6 – 7 K lower than the mean temperatures estimated with the first method. This finding is reasonable because the mean temperature is an average for the envelope temperature. André & Montmerle (1994) expressed the averaged temperature of the envelope as

$$\overline{T} \simeq (3 - p/3 - p - q)\, T_{\rm ext} \quad (5)$$

which, for the adopted values of p and q (1.5 and 0.3 respectively), gives $\overline{T}/T_{\rm ext}$ = 1.25. This brings the external temperatures determined with the shell model in excellent agreement with the average temperatures obtained using Eq. 1.

Therefore, we believe that the assumption of a homogeneous isothermal dust sphere adopted in Eq. 1 is a viable approach for a reliable estimate of the dust mass and temperature; this result, valid for Class 0 sources (Ward-Thompson et al. 1995), is verified here for Class I sources.

3.4. The value of κ_0

The value of κ_0, the normalisation factor of the dust opacity law at 250 μm, is poorly known, mainly due to uncertainties in grains structure (Colangeli et al. 1995; Ossenkopf & Henning 1994). Laboratory measurements and theoretical calculations agree better if a CDE (Continuous Distribution of Ellipsoids) model is used (Colangeli et al. 1995).

According to Reipurth et al. (1993), the value of κ(1.3 mm) is in the range 3 10^{-3} to 2 10^{-2} cm^2/g. Using our β values in the range 1.1 – 1.9 and taking κ_0=0.1 cm^2/g, we find κ(1.3 mm) in the range 4.4 10^{-3} to 1.7 10^{-2} cm^2/g, in good agreement with the above values (see also Ossenkopf & Henning 1994).

To better constraint the value of κ_0, we estimated, in an independent way, a total mass for the L1641 sources: $M_{\rm H_2}$ ($M_\odot$) = 0.025 A_V (see Walker et al. 1990), using A_V values given by SNS and Chen & Tokunaga (1994) and assuming the circumstellar material to be distributed in a sphere (R=$R_{\rm beam}$=10″). Results are presented in Table 4. Column 2 gives the visual extinction value. The third column gives the mass, assuming spherical geometry. Column 4 gives the mass ranges determined using Eq. 1.

A general agreement is found between the two mass determinations, supporting the chosen κ_0 value. This method does not allow us to give a precise value for κ_0 but indicates that a high value (leading to relatively low masses; see Eq. 1) is needed to obtain an agreement between the two independent mass estimates.

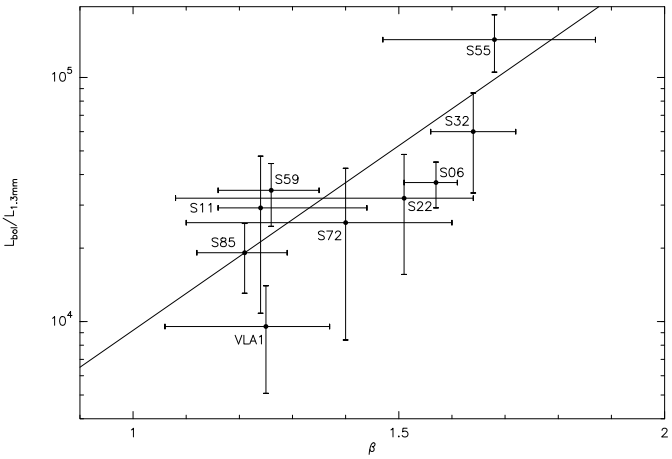

Fig. 2. The bolometric-to-1.3 mm luminosity ratio versus β. The solid line is the best-fit log($L_{\rm bol}/L_{1.3\,\rm mm}$)=1.32$\beta$+2.635, with a 95.5% correlation probability

Table 4. Independent mass estimate

Name	A_V	$M_{\rm H_2}$	$\overline{M}$
			($M_\odot$)
S06	>60	> 1.5	3.5 - 4.3
S11	32	0.8	0.6 - 1.06
S22	45	1.1	0.38 - 1.08
S32	48	1.2	0.74 - 1.02
S55	33	0.8	0.32 - 0.72
S59	53	1.3	1 - 1.5
S72	40	1	0.28 - 0.66
S85	43	1.05	0.29 - 0.4
VLA1	>60	> 1.5	0.87 - 1.61

4. The change of β with time

André et al. (1993) suggested the use of the ($L_{\rm bol}/L_{1.3\,\rm mm}$) ratio as an evolutionary indicator for pre-main-sequence objects because, during this phase, the circumstellar mass, proportional to $L_{1.3\,\rm mm}$, is expected to decrease, disappearing when the object reaches the main-sequence. As a consequence of this, older sources will have a higher ($L_{\rm bol}/L_{1.3\,\rm mm}$) value.

In Fig. 2 we plot the objects of our sample in a ($L_{\rm bol}/L_{1.3\,\rm mm}$) versus β diagram. We see a trend towards a correlation between the two plotted quantities and the best-fit log($L_{\rm bol}/L_{1.3\,\rm mm}$)= 1.32 β+2.635 (solid line) gives a correlation probability of 95.5%.

Fig. 2 also shows that sources with a high value of $L_{\rm bol}/L_{1.3\,\rm mm}$ (older sources) also tend to have a higher β value. Therefore, β seems to increase with time. Dent et al. (1995), using a submillimetre colour-colour diagram, also noted an increase of β, associated with an increase in the dust temperature, as the sources evolve. Our sources, superimposed on their diagram (their Fig. 1b), follow the same trend of a colour-colour increase as time proceeds (older sources have higher temperatures and higher β, see Table 2). They interpreted the observed evolution as being due to a change in dust properties. A temper-

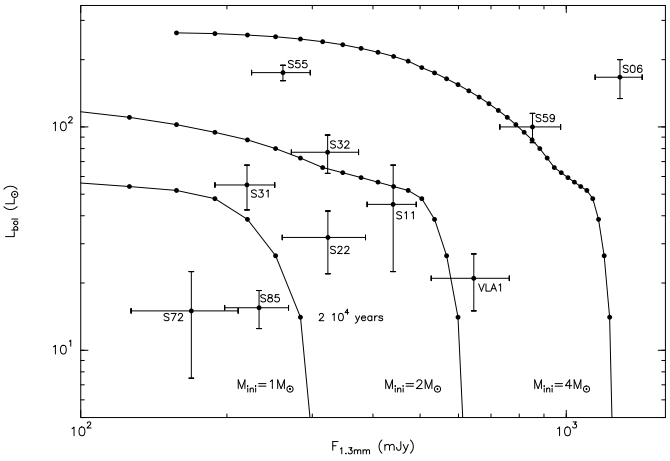

Fig. 3. Bolometric luminosity, $L_{\rm bol}$, versus the 1.3 mm flux, $F_{1.3\,\rm mm}$. Evolution tracks are shown for initial mass envelopes of 1, 2 and 4 $M_\odot$ and a constant mass accretion rate of $\dot{M}$=10^{-5} $M_\odot$/year. The first (lowest) points are for 2 10^4 years. Each subsequent point represents a time step of 10^4 years

ature increase during the source evolution can change the dust structure (destruction of ice mantles and compact structures). This agrees with the observed evolution of the dust opacity law (Ossenkopf & Henning 1994), $\kappa(\lambda)$, which changes from $\lambda^{-1.2}$ to $\lambda^{-1.9}$ (respectively for small silicate grains with a coating of amorphous carbon with an ice mantle, and for small silicate grains with separated amorphous carbon grains). The flatter submillimetre spectrum observed for Class 0 sources (Ward-Thompson et al. 1995) could be interpreted as being due to the presence of larger grains in their envelopes, well expressed by a lower β value (Krügel & Siebenmorgen 1994; Dent et al. 1995).

Another indication of the possible evolution of β is shown in Fig. 3. We have plotted our data in a bolometric luminosity ($L_{\rm bol}$) versus millimetre flux ($F_{1.3\,\rm mm}$) diagram (Saraceno et al. 1996). In such a diagram, Saraceno et al. (1996) plotted evolutionary tracks for accreting objects. Each track originates from an envelope of initial mass of dust and gas that produces objects of different masses. The dust temperature and opacity law are fixed (T=25 K, β=1.5; see their Sect. 5.4 for further details). The points on the lines correspond to a constant time step of 10^4 years.

From Fig. 3, we can propose an evolutionary sequence from younger to older sources: VLA1, S11, S32 and S55. The corresponding β increases with time (from 1.25 for VLA1 to 1.68 for S55). Moreover, even if in this scheme objects have different masses, we can say that S22 (β=1.51) is older than VLA1 (β=1.25) and S85 (β=1.21) or that S55 (β=1.68) is older than S59 (β=1.26). This indicates that β may increase with time.

The increase in β produces a steeper slope of the continuum as the source evolves. This shape indirectly influences the determination of the bolometric luminosity, i.e. objects with similar $F_{1.3\,\rm mm}$ but with a higher β will have a higher bolometric luminosity (see for example the cases of S22 and S32 or S55 and S85 in Fig. 3). Therefore, the possible evolution of β (traducing a change in dust properties) could influence the increase of the ($L_{\rm bol}/L_{1.3\,\rm mm}$) ratio.

Two other points give further indications in favour of an evolution of β with time.
Due to their sharply peaked spectral energy distributions, Class I sources of our sample show a proportionality between their 100 μm flux and their bolometric luminosity. Therefore we have

$$L_{\rm bol}/L_{1.3\,\rm mm} \propto F_{100\,\mu\rm m}/F_{1.3\,\rm mm}. \quad (6)$$

Moreover, using Eq. 1, we can also write

$$F_{100\,\mu\rm m}/F_{1.3\,\rm mm} \propto 13^{3+\beta} f(T), \quad (7)$$

with $f(T) \propto (e^{11/T}-1)/(e^{144/T}-1)$. Equations (6) and (7) show that the ($L_{\rm bol}/L_{1.3\,\rm mm}$) ratio is a function of T and β and we see that β increases with this ratio. As a direct consequence, if we fix the same temperature for all the source and use Eq. 1 taking only the submillimetre points, we find β values that also increase with the $L_{\rm bol}/L_{1.3\,\rm mm}$ ratio.
Because as time proceeds the envelope material is dispersed or accreted, the decrease of the 1.3 mm flux is an evolutionary indicator. Using the time sequence seen in Fig. 3, we can make an $F_{1.3\,\rm mm}$ - β diagram. On such a diagram, in a given class of mass defined by the intensity of the 1.3 mm flux, the β value (obtained with the least-squares fit) increases as the flux diminishes. This last point also indicates a possible evolution of β as time proceeds.

5. Conclusions

We have presented a 60 μm – 1.3 mm continuum study of ten Class I sources in the L1641 cloud. Our main findings are:
(i) for Class 0 and Class I sources, the use of the Hildebrand formula is a good way to obtain the circumstellar mass and β, because a single temperature greybody reproduces well the observed continuum;
(ii) the exponent of the dust opacity law, β, seems to increase with time, contributing to the evolution of the ($L_{\rm bol}/L_{1.3\,\rm mm}$) ratio.

The possible evolution of β with time clearly needs further investigation, especially in the mid-IR and submillimetre ranges to search for possible change in dust properties.

Acknowledgements. A. Zavagno is grateful for the support of an ESA external fellowship and thanks J. Caplan for his careful reading of the manuscript. D. Lorenzetti and P. André are thanked for many fruitful discussions. The authors would like to thank the James Clerk Maxwell Telescope staff, in particular Wayne Holland, for their assistance during the observations. The James Clerk Maxwell Telescope is operated by The Observatories on behalf of the UK PPARC, the Canadian NRC and the Netherlands ZWO. This research has made use of the Simbad database, operated at CDS, Strasbourg, France.

Appendix A

A.1. Observed emission excess around 1.3 mm

As mentioned in Table 1, S22 and VLA1 show a 1.3 mm excess compared to the obtained fit (see Fig. 1). Extended emission is excluded as the 1.3 mm beam size is not significantly larger than the others. Possible calibration error has been searched for and excluded. Some other sources in our sample are also studied by Reipurth et al. (1993) and measurements are in good agreement, within the error bars. Radio continuum emission has been measured for 67 objects of the L1641 molecular cloud (Morgan et al. 1990). Fluxes at 6 and 20 cm were used to evaluate the expected free-free emission at 1.3 mm. In two cases, this contribution is negligible (less than 0.2% of the 1.3 mm flux; see also Walker et al. 1990). Therefore, free-free emission cannot be responsible for this excess. New measurements are needed to confirm the observed excesses.

A.2. Discussion of individual sources

Some sources in our sample have a complicated morphology not resolved by IRAS (see Pravdo & Chester 1987) and this can affect the determination of the parameters. To estimate the fit reliability, we have investigated evidence for IRAS confusion.

– **S06 - L1641-N**
In the near IR, this source is a cluster of objects but one is dominant (see Chen et al. 1993a) and coincides with the the 2.7 mm peak (Wilking et al. 1990).
The parameters obtained for this source do not agree with those obtained for the rest of the sample. The fit tends to pass through the upper limits of the submillimetre measurements (see Fig. 1). This is also revealed by the difference in β values between S59 and S06, two sources which have similar ($L_{\rm bol}/L_{1.3\,\rm mm}$) values (see Fig. 2) and which should be in a similar evolutionary stage, if one considers that their initial envelope masses are not too different. S06 is also the only source associated with a relatively low dust temperature (see Table 2) considering its 100 μm flux. Finally, the fit obtained using its associated IRAS-PSC fluxes (lower than those determined by SNS) gives T=34.7 K, β=1.25 and M=2.1 $M_{\odot}$, similar to those obtained for S59. Moreover, if we fix the same temperature for S06 and S59 (see also Reipurth et al. 1993), an agreement is found between the two sets of obtained parameters. Finally, we found no evolutionary track (with an accretion rate of 10^{-5} $M_{\odot}$/year) that reproduces the observed quantities for S06 (see Fig. 3). We think that extension and clustering in this source lead to an overestimate of the fluxes. For consistency, we have kept the parameters obtained with the least-squares fit, but point out possible problems.

– **S11 - MSSB-8**
The multiple components of this source were not resolved by IRAS (Chen & Tokunaga 1994; SNS). However, we consider the fit to be reliable (see Sect. 3.2).

– **S22 - MSSB-18**
This source exhibits no clear near IR counterpart (see Fig. 2 in Chen & Tokunaga 1994). The source is seen at longer wavelengths to the south of the IRAS position (SNS), in agreement with the observed displacement of the submillimetre peak. We consider the fit to be reliable. Due to the observed excess, we excluded the measured 1.3 mm flux from the fit procedure and took the one which agrees with the fit for all the quantities linked to it. The great similarity of the measured submillimetre continuum fluxes of this source with those of S32 shows the reliability to this procedure.

– **S31**
This source, together with S32 and VLA1, is found in a confused region (Pravdo & Chester 1987) which renders the association between IRAS and submillimetre fluxes highly doubtful. Therefore, we excluded this source from the analysis.
An upper limit for the bolometric luminosity obtained using available IRAS-PSC fluxes is given in Table 1. As tested by our fit procedure, these fluxes are also too high to be associated with the submillimetre measurements. However, the use of an upper limit for the bolometric luminosity allow us to discuss some properties of this source.
The submillimetre spectral slope of S31 is very similar to that of other sources of our sample and, apart from an overestimate of its IR fluxes, we think that its nature as a Class I source is not in question.

– **S32 - MSSB-21**
At 100 μm, this source is the dominant component of a blend (SNS), so the flux may be overestimated. As for the previous source, the fluxes obtained by Chen et al. (1993b) lead to unrealistic β values. We consider the fit to be reliable (see Fig. 1).

– **S55 - L1641-S**
This source is associated with a strong nebulosity in the near IR (see Chen & Tokunaga 1994) and lies on a broad pedestal in the four IRAS bands (SNS), giving the unusual shape of its IR spectrum for a Class I source. Cohen (1990) determined IR fluxes and we run our fit procedure, with consistent results (high values for T and β). Moreover, fixing the same dust temperature (in the range 25 – 35 K) for all the sources (see also Reipurth et al. 1993), we performed a least-squares fit using only the submillimetre points and found that S55 remains the most evolved source of our sample. Therefore we consider the fit to be reliable. Our 1.3 mm measurement agrees with that of Reipurth et al. (1993).

– **S59 - L1641-S3**
This strong submillimetre source is relatively isolated and has well determined IR fluxes. We consider the fit to be reliable.

– **S72**
Even though there are large errors in the parameters values due to large errors in the 100 μm flux, we consider the fit to be reliable.

– **S85 - L1641-S4**
This source lies in a confused region. The 60 and 100 μm fluxes measured by Chen et al. (1993b) are associated with

100% uncertainty. Fluxes determined by SNS and the PSC agree. We consider the fit to be reliable.

– **VLA1**
This strong millimetre source is located near S31 and S32 and has no near IR counterpart (see Chen & Tokunaga 1994). Due to confusion, no IRAS fluxes have been determined. We took the 50 and 100 μm fluxes from Harvey et al. (1986). Our 1.3 mm measurement agrees with that of Reipurth et al. (1993), within the errors. Their 870 μm and 1.3 mm flux measurements are shown in Fig. 1.

References

Adams F.C., 1991, ApJ 382, 544
André P., Ward-Thompson D., Barsony M., 1993, ApJ 406, 122
André P., Montmerle T., 1994, ApJ 420, 837
Cabrit S., André P., 1991, ApJ 379, L25
Cardelli J.A., Clayton C., Mathis J.S., 1989, ApJ 345, 245
Chen H., Tokunaga A.T., Strom K.M., Hodapp, 1993a, ApJ 407, 639
Chen H., Tokunaga A.T., Fukui Y., 1993b, ApJ 416, 235
Chen H., Tokunaga A.T., 1994, ApJS 90, 149
Cohen M., 1990, ApJ 354, 701 (erratum: ApJ 362, 758)
Colangeli L., Mennella V., Palumbo P., Rotundi A., Bussoletti E., 1995, A&A 303, 976
Correia J.C., Griffin M., Saraceno P., Zavagno A., 1996, in ESO Workshop Series: "The role of dust in the formation of stars", p. 11, eds. Siebenmorgen R. & Kaulf H.U., (Springer-Verlag)
Davis C.J., Eislöffel J., 1995, A&A 300, 851 (erratum: A&A 305, 694)
Dent W.R.F., Matthews H.E., Ward-Thompson D., 1995, Ap&SS 224, 85
Ducan W.D., Robson E.I., Ade P.A.R., Griffin M.J., Sandell G., 1990, MNRAS 243, 126
Harvey P.M., Marshall J., Lester D.F., Wilking B.A., 1986, ApJ 301, 346
Henning Th., 1983, Ap&SS 97, 405
Henning Th., Launhardt R., Steinacker J., Thamm E., 1994, A&A 291, 546
Hildebrand R. H., 1983, QJRAS 24, 267
IRAS Point Source Catalog, 1988, Joint IRAS Science Working Group (Washington, DC:GPO) (PSC)
Krügel E., Siebenmorgen R., 1994, A&A 288, 929
Lada C.J., 1987, in I.A.U Symposium n°115: "Star Forming Regions", p. 1, eds. M. Peimbert & J. Jugaku, (Dordrecht: Reidel)
Lada C.J., 1991, in "The Physics of Star Formation and Early Stellar Evolution", p. 329, eds. C.J. Lada & N.D. Kylafis (Dordrecht: Kluwer)
Mannings V., Emerson J.P., 1994, MNRAS 267, 361
McMullin J.P., Mundy L.G., Blake G.A., 1994, ApJ 437, 305
Morgan J.A., Snell R.L., Strom K.M., 1990, ApJ 362, 274
Morgan J.A., Bally J., 1991, ApJ 372, 505
Morgan J.A., Schloerb F.P., Snell R.L., Bally J., 1991, ApJ 376, 618
Myers P.C., Fuller G.A., Mathieu R.D., Beichman C.A., Benson P.J., Schild R.E., Emerson J.P., 1987, ApJ 319, 340
Ossenkopf V., Henning T., 1994, A&A 291, 943
Pravdo S.H., Chester, T.J., 1987, ApJ 314, 308
Reipurth B., Chini R., Krügel E., Kreysa E., Sievers A., 1993, A&A 273, 221
Sandell G., 1994, MNRAS 271, 75
Sakamoto S., Hayashi M., Hasegawa T., Handa T., Oka T., 1994, ApJ 425, 641
Saraceno P., André P., Ceccarelli C., Griffin M., Molinari S., 1996, A&A 309, 827
Seab C.G., 1987, in "Interstellar Processes", p. 491, eds. D.A. Hollenbach & H.J. Thronson (Dordrecht: Reidel)
Strom K.M., Newton G., Strom S.E., Seaman R.L., Carrasco L., Cruz-Gonzalez I., Serrano A., Grasdalen G.L., 1989, ApJS 71, 183 (SNS)
Walker C.K., Adams F.C., Lada C.J., 1990, ApJ 349, 515
Ward-Thompson D., Chini R., Krügel E., André P., Bontemps S., 1995, MNRAS 274, 1219
Wilking B.A., Blackwell J.H., Mundy L.G., 1990, AJ 100, 758

This article was processed by the author using Springer-Verlag LaTeX A&A style file *L-AA* version 3.